Ocean and Coastal Management xxx (xxxx) xxx

Contents lists available at ScienceDirect

Ocean and Coastal Management

journal homepage: http://www.elsevier.com/locate/ocecoaman

Morphodynamic couplings between the Biandan Shoal and Xinqiao Channel, Changjiang (Yangtze) Estuary

Yaying Lou [a], Zhijun Dai [a,b,*], Yuying He [a], Xuefei Mei [a], Wen Wei [a]

[a] State Key Lab of Estuarine & Coastal Research, East China Normal University, Shanghai, 200062, China
[b] Laboratory for Marine Geology, Qingdao National Laboratory for Marine Science and Technology, Qingdao, 266100, PR China

ARTICLE INFO

Keywords:
Shoal-channel system
Morphodynamic process
Anthropogenic activities
Changjiang (Yangtze) Estuary

ABSTRACT

Channel-shoal systems (CSS) are some of the significant morphodynamic cells in estuaries, which provide immeasurable economic, ecological and environmental value. However, most CSS in mega-estuaries of the world are facing great challenges from serious risk of degradation due to intensive human activities and sea-level rise. Here, we focus on the tradeoff between the Biandan Shoal (BDS) and Xinqiao Channel (XQC), which is the largest CSS of the South Branch, Changjiang Estuary. The results show that the BDS area above the 5 m water depth had an observable increasing tendency with an interannual increasing rate of 1.43 km^2/yr during 1996–2016. The corresponding XQC volume exhibited an obvious reduction trend with an annual decreasing rate of 3.79×10^6 m^3/yr. Meanwhile, the BDS presented lateral and downward extension with more than 4.7 km of downward movement, while the XQC indicated shrinking with the width of the upper reaches decreasing by nearly half since 1998. Furthermore, the morphodynamic evolution of the BDS-XQC system during 1998–2016 could be divided into four stages: preflood stage with the joint extension of the BDS and XQC (1996–1998); conversion stage due to impacts from the extreme flood (1998–2000); development stage with obvious deposition throughout the system (2000–2009); stabilization stage with deposition on the high flats but no lateral expansion of the BDS, and continuous shrinkage of the XQC (2009–2016). The dynamic balance of the BDS-XQC system was mainly determined by the tradeoffs between the BDS and XQC, even though the occasional extreme hydrological events disrupted the coupling of the BDS-XQC. Meanwhile, the local channel blocked by the construction of the Dongfengxisha Reservoir induced a decrease in water discharge into the XQC, which was responsible for the recent XQC recession. In light of the impact of future climate change and increasing human interference in the anthropogenic era, fragile CSS distributed in estuaries should be holistically considered with policies to support sustainable integrated coastal zone management.

1. Introduction

Channel-shoal systems (CSS) are ubiquitous geomorphologic features in most estuaries of the world (Barua, 1990). These systems play an important role in navigation, ecology and land reclamation, which are key factors in sustaining regional socioeconomic and environmental development (Schuttelaars and De Swart, 1997; Hibma et al., 2004; Brake and Schuttelaars, 2011). However, estuarine CSS have undergone dramatic degradation worldwide in response to natural and increasing anthropogenic interferences (Lafite and Romaña, 2001; Anthony et al., 2014; van et al., 2015). Thereafter, understanding the morphodynamic of CSS is crucial for the comprehension of holistic estuarine evolution, the management of estuarine ecological environments, and the development of related policy regulations.

The earliest studies of CSS were derived from Van Veen's observation work in the Westerschelde Estuary of the Netherlands (Van Veen, 1950). This study revealed that there were different meander configurations for CSS, including flood- and ebb-based channels, which are isolated with shoal separation (Van Veen, 1950). Subsequently, Robinson (1956) further improved Van Veen's work and considered that a flood channel would be deeper than an ebb channel when the flood stream was stronger than the ebb. However, in areas where the maximum velocities of flood and ebb streams were nearly equal or where the ebb was considerably strengthened by river water, flood channel would be shallower than the ebb channel (Robinson, 1956). Dyer (1977) suggested that the formation of flood and ebb channels could result from the

* Corresponding author. State Key Lab of Estuarine & Coastal Research, East China Normal University, Shanghai, 200062, China.
E-mail addresses: 52183904012@stu.ecnu.edu.cn (Y. Lou), zjdai@sklec.ecnu.edu.cn (Z. Dai).

https://doi.org/10.1016/j.ocecoaman.2019.105036
Received 23 January 2019; Received in revised form 28 September 2019; Accepted 21 October 2019

channel divergence induced by the inconsistent flow path. The evolution of CSS was the coeffect of multiple factors, including tides, waves and runoff (Dyer, 1977). Later, Schuttelaars and De Swart (1997) found that channel-shoal formation, as observed in short tidal embayments, could be explained by a positive feedback mechanism between the tidal flow and the bottom. Levinson and Atkinson (1999) proposed that the Coriolis force affect the distribution of the flow field in the flood channel of the Chesapeake Estuary. Hibma et al. (2004) investigated the dominant wavelengths of CSS together with their dependency on the width and depth of the basin and the local maximum velocity. A series of studies also indicated that the evolution of CSS in macro-tidal and meso-tidal estuaries was closely connected with tidal and fluvial actions, such as those in the Ganges-Brahmaputra-Meghnahna Estuary (Barua, 1990), Qiantang Estuary (Yu et al., 2012; Xie and Pan, 2013), and Apalachicola Bay (Leonardi et al., 2015).

Recently, Kleinhans et al. (2015) demonstrated the dynamic equilibrium and quasiperiodic behavior of the CSS, which are intrinsic characteristics and do not require external forcing. Nevertheless, extreme events (Darby et al., 2013; Dai et al., 2016) and anthropogenic activities (Wal et al., 2002; Jeuken and Wang, 2010) affected these characters in nature. In particular, anthropogenic interventions have revolutionized the natural development of CSS in recent decades (Dabees and Kraus, 2008; Hibma et al., 2008). Examples can be seen in estuaries worldwide: in the Ribble Estuary, northwest England, the ebb flow concentrated in the over-deepened channel, heightening sedimentation because of dredging activities (Wal et al., 2002). In the Westerschelde Estuary, due to the strong intensity of dredging-dumping activities, the stability of the natural ebb-flood channel system broke, and the system turned into a single channel (Jeuken and Wang, 2010). Afterwards, in Qinzhou Bay, Wang et al. (2014) found that dredging throughout the full length of the ebb-dominated east channel could trigger long-term erosion in other ebb-dominated channels, which contributed to the stability of the channel-shoal system. Although some studies provided an understanding of how the combination of natural forcings and anthropogenic activities affected CSS morphodynamics, few studies have focused on CSS evolution under the coupling effects of both river basin interference and estuarine engineering projects, especially in mega-estuaries, such as the Changjiang Estuary.

The Changjiang Estuary (Fig. 1b), with a length of 120 km and a width of 90 km at its outer limit, is the largest bifurcated estuary in Asia (Chen et al., 1979; Mei et al., 2018a). The estuary is, being divided by three islands, Chongming, Hengsha, and Jiuduan Shoal, and is characterized by four branches of tidal channels and three major bifurcations (Dai et al., 2015) (Fig. 1b). Like any other large estuary in the world, it possesses plenty of channel-shoal geomorphic systems (Liu et al., 2004a, b; Wei et al., 2016). Among them, the Biandan Shoal (BDS) and Xinqiao Channel (XQC) in the South Branch near Chongming Island are defined as a typical channel-shoal system (Chen and Xu, 1981) (Fig. 1b).

The BDS, which is located in the lower reaches of the Baimao Shoal, is the largest mid-channel bar of the South Branch. The length of the BDS is approximately 37 km, and the area enclosed by 5 m isobaths is approximately 100 km^2. The BDS is further divided into the Upper Biandan Shoal (UBDS) and Lower Biandan Shoal (LBDS) (Fig. 1b). The UBDS is the northern boundary of the lower segment of the Baimao Shoal North Waterway (Fig. 1b). As the largest untouched shoal in the South Branch, the BDS has great potential in terms of land-use and the ecological environments. Meanwhile, as it is located in the central area of a group of reservoirs in the Changjiang Estuary, the evolution of the BDS may affect the water resource utilization and management throughout the estuary. The XQC is on the north side of the BDS, which is a flood channel between the BDS and Chongming Island. The channel, extending 35 km from Miaogang to Baozhen, is the longest flood channel in the South Branch (Fig. 1c). The XQC is an essential channel in the Changjiang Estuary, which is not only responsible for navigation, but also the fresh water source for Chongming Island (Wang et al., 2005). However, the effects of natural and anthropogenic interferences on the

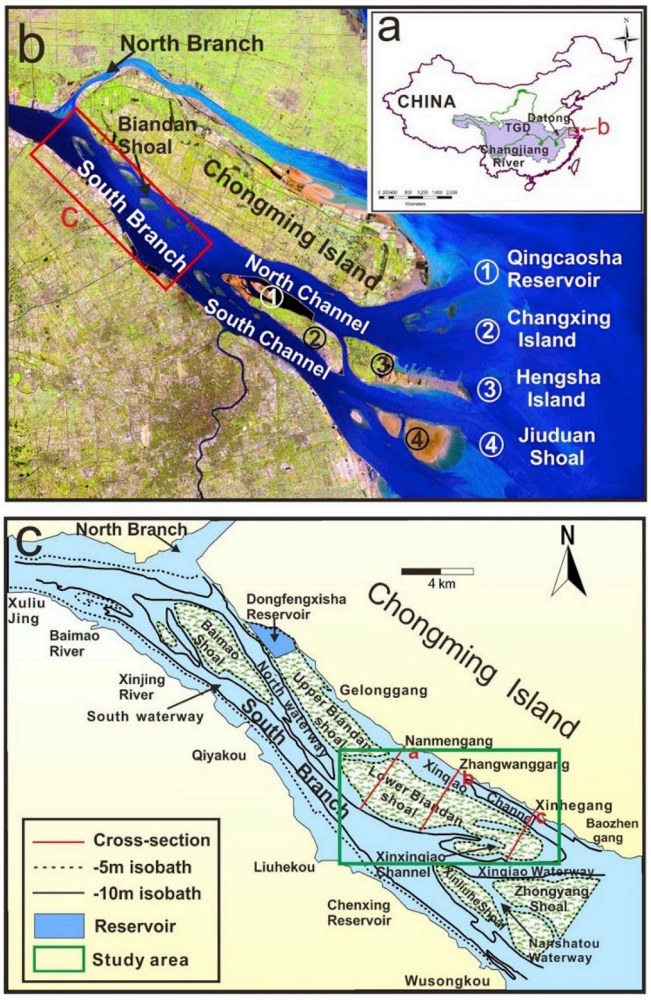

Fig. 1. Map showing the study area, with the Changjiang River and the location of the Three Gorges Dam and Datong station; b Changjiang Estuary; c the BDS-XQC system.

BDS-XQC system remain to be explored. Moreover, unlike the UBDS, the LBDS is currently in the turbulence stage due to the lack of artificial engineering protection. Therefore, in this study, we focus on the LBDS and the XQC from Nanmengang to Baozhen (Fig. 1c). The main aims of this paper are to (1) explore the variations in the BDS-XQC system in recent decades; (2) discern the morphodynamic patterns of the BDS-XQC system; and (3) diagnose the possible impacts from natural and anthropogenic forcing that dominate the BDS-XQC evolution.

2. Data and methods

2.1. Data collection

Bathymetric data are invaluable for quantitative research of estuarine morphodynamic evolution (van and Pye, 2003; Blott et al., 2006; Carbonneau et al., 2010). The bathymetric charts, covering the XQC and LBDS area in uneven intervals over the period from 1996 to 2016, were collected from different sources of officially published materials (Table 1). Specifically, the charts from 1996 to 1998 were monitored by the Safety Supervision Bureau, Ministry of Communications of China, while those from 1999 to 2016 were provided by the Maritime Safety Administration of People's Republic of China (Table 1). Water depth was observed by dual-frequency echo sounders with a vertical error of 0.1 m (Wei et al., 2016). The chart scale is 1:25,000 with a data density of 8–15 points per km^2.

Table 1
Details about the bathymetric data of the North Channel, Changjiang Estuary.

Survey data	Scale	Data source
1996; 1997; 1998	1:25000	SSBMC
1999; 2000; 2001; 2002; 2004; 2005; 2007; 2009; 2014; 2015; 2016	1:25000	MSAC

Note: SSBMC: Safety Supervision Bureau, Ministry of Communications of China. MSAC: Maritime Safety Administration of People's Republic of China.

Meanwhile, yearly runoff and suspended sediment discharge (SSD) during 1996–2014 at the Datong station (the most downstream hydrologic station in the Changjiang River) were collected to explore the impacts of riverine fluxes on the evolution of the BDS and XQC. These data were obtained from the Changjiang Water Resources Commission.

2.2. Bathymetric data processing methods

Bathymetric data spanning the period 1996–2016 were digitized with ArcGIS 10.4 to acquire a series of data for further analysis. Raw bathymetric data were first converted to elevation relative to Beijing-1954 coordinates and corrected to the 'Wusong Datum'. Subsequently, the bathymetric data were gridded with 20 × 20 m cells to build a digital elevation model (DEM) using the kriging interpolation method. In addition, all the isobaths, including 0 m, 5 m, and 10 m, were directly extracted from the charts and transformed into Beijing-1954 coordinates. Thereinto, the area with a water depth above 0 m represents the high floodplain area of the LBDS. The 5 m isobaths are the boundary between the shoal and channel, whose envelope scope represents the superficial area of LBDS. 10 m isobaths are correlated to the XQC morphology (Wei et al., 2017). To detect the geomorphologic variability of the BDS-XQC system, three transverse sections that dominate the upstream, midstream and downstream evolution were extracted from the DEM. The location of each cross-sectional is shown in Fig. 1. Meanwhile, the deposition and erosion patterns were obtained by subtracting the two subsequent morphological surveys.

2.3. Fractal analysis

In recent decades, fractal analysis has been applied extensively in geography research, such as evolution analysis (Mandelbrot, 1967), segmentation research (Voorons et al., 2003) and pattern recognition (Dai et al., 2018a). The main characteristic of fractal geometry is the ability to describe the irregular or fragmented shapes of natural features as well as other complex objects that are difficult to analyze in traditional ways (Lopes and Betrouni, 2009). In this paper, fractal analysis was used to present the evolution of the BDS-XQC system directly and quantitatively. The fractal dimensions D of the BDS contour lines in different years were measured using the box counting method (Feder, 1988). The estimation of D was carried out through the following steps:

(1) A series of square grid sequences with uniform length S are established to cover the entire image. The number of boxes N with length S that contain the BDS contour lines are counted. Different grid sizes *(S)* can generate different numbers of boxes *(N)*.
(2) The value of D is estimated theoretically by Rinaldo et al., 1993:

$$D = \lim_{S \to 0} \frac{\log N(S)}{\log\left(\frac{1}{S}\right)} \tag{1}$$

(3) The correlation between $N(S)$ and $1/S$ is quantified by linear regression. The fractal dimension D is the slope of the obtained regression line.

2.4. Grey relational analysis

Furthermore, to explore the impacted factors of the XQC river volume, grey relational analysis (GRA) was applied, which is a classical statistical technique in geography, social systems, ecological systems and environmental studies (Wen, 2004). The theory of GRA is to calculate the similarity degree of development trends among factors, which is appropriate for solving the complicated interrelationships between multiple factors and variables (Morán et al., 2006). It puts forward the grey relational coefficient to measure the correlation between factors. The GRA algorithm can be described in detail as follows (Wen, 2004; Morán et al., 2006; Kuo et al., 2008):

Standardization: When it is necessary to compare a series of influencing factors with different units, variable standardization is a favorable approach.

$$X_{ij} = \frac{Y_{ij} - min_j Y}{max_j Y_{ij} - min_j Y_{ij}} \tag{2}$$

where Y_{ij} is the jth influence factor in the ith year.

Correlation coefficient (ε): As a reference sequence has several comparability sequences, the calculated correlation coefficient (ε) between each comparability sequence and reference sequence at each time can be calculated as:

$$\varepsilon_i(j) = \frac{min_i max_j |X_0(j) - X_i(j)| + \delta max_i max_k |X_0(j) - X_i(j)|}{|X_0(j) - X_i(j)| + \delta max_i max_k |X_0(j) - X_i(j)|} \tag{3}$$

where X_0 is the reference sequence, which is characterized as the volume of XQC in this study, and X_i is the comparability sequence, which is the influence factor of XQC. δ is an identification coefficient $(0 < \delta < 1)$, which was initially set as 0.5 in this study.

Grey relational grade (r_i): the mean of the grey correlation coefficient. Since the correlation coefficients is too scattered to make an overall evaluation, we centralize the correlation coefficient each moment to a value through the grey relational grade formulation:

$$r_i = \frac{1}{N} \sum_{j=1}^{N} \varepsilon_i(j) \tag{4}$$

where j is the number of variables, and N is the number of years.

As mentioned above, the relation between the volume of XQC and different effect factors can be precisely quantified through GRA. The effect factors obtain the highest grey relational grade (r_i) with the XQC volume, showing they are most relevant to XQC's development (Kuo et al., 2008).

3. Results

3.1. Morphodynamics of LBDS

Estuarine isobaths are effective tools to reflect morphodynamic changes, which have been widely applied in geographic, ecological and environmental studies (Macdonald et al., 1990; Liu et al., 2004a,b). In view of the geographic features of the BDS, the configuration of the UBDS has remained relatively stable in recent decades (Yun, 2004). Here, the BDS morphological variations are primarily concentrated on the LBDS. The 0 m and 5 m isobaths of the LBDS exhibited a series of distinct morphological variations from 1996 to 2016 (Fig. 2)There was an obvious rising trend in the 0 m isobaths of the LBDS, with the interannual increasing rate reaching 1.08 km^2 (Fig. 2a), showing that the area of the high floodplain increased gradually from 1996 to 2016. Specifically, the high floodplain area above 0 m was approximately 10 km^2 in 1996, which increased to 31 km^2 in 2015. Meanwhile, the high floodplain indicated over 7.5 km of downward movement between 1996 and 2015. Particularly, in 1998, the LBDS moved downward significantly by more than 2 km compared with that in 1996 (Fig. 3a).

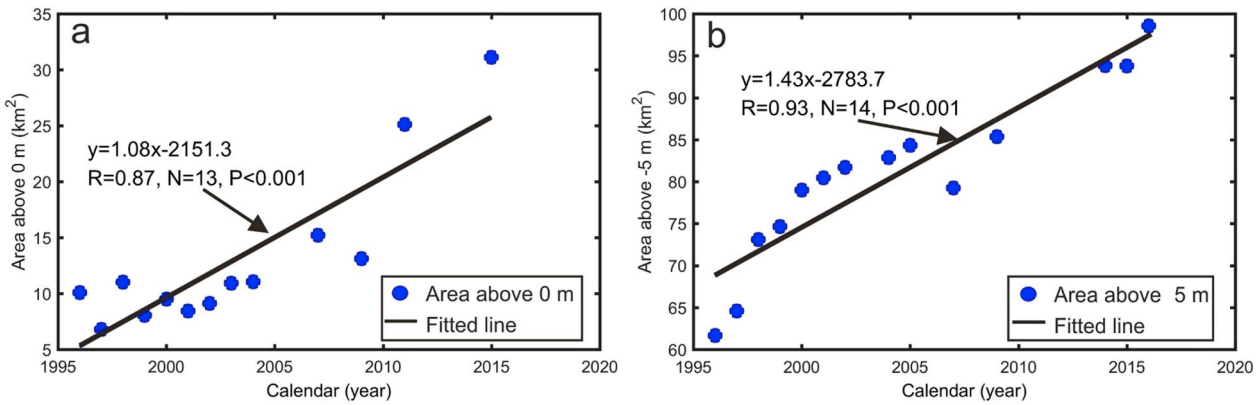

Fig. 2. Area changes in LBDS, with a above 0 m; b above 5 m.

Moreover, there were clear variations in the 0 m configurations during 1996–2016. In 1996, the intertidal zone was approximately elliptically shaped and gradually transformed into jagged formations in the following 6 years. The jagged intertidal zone became distinct after 2004 and formed a multifinger shape through breakdown and combination (Fig. 3), which developed to be relatively stable thereafter.

In comparison with the variations in 0 m isobaths, 5 m isobaths, representing LBDS's surface morphology, exhibited more disciplinary. Since 1996, LBDS has shown clear lateral and downward extensions in isobath movements. The area with a water depth above 5 m increased by 1.5 times from 61 km^2 in 1996 to 98 km^2 in 2016 (Fig. 2b). Meanwhile, 5 m isobaths extended seaward by over 4.7 km (Fig. 4). In brief, the surface morphology of LBDS changed from the original elongation to a multifinger shape under the effects of surrounding shoals and troughs

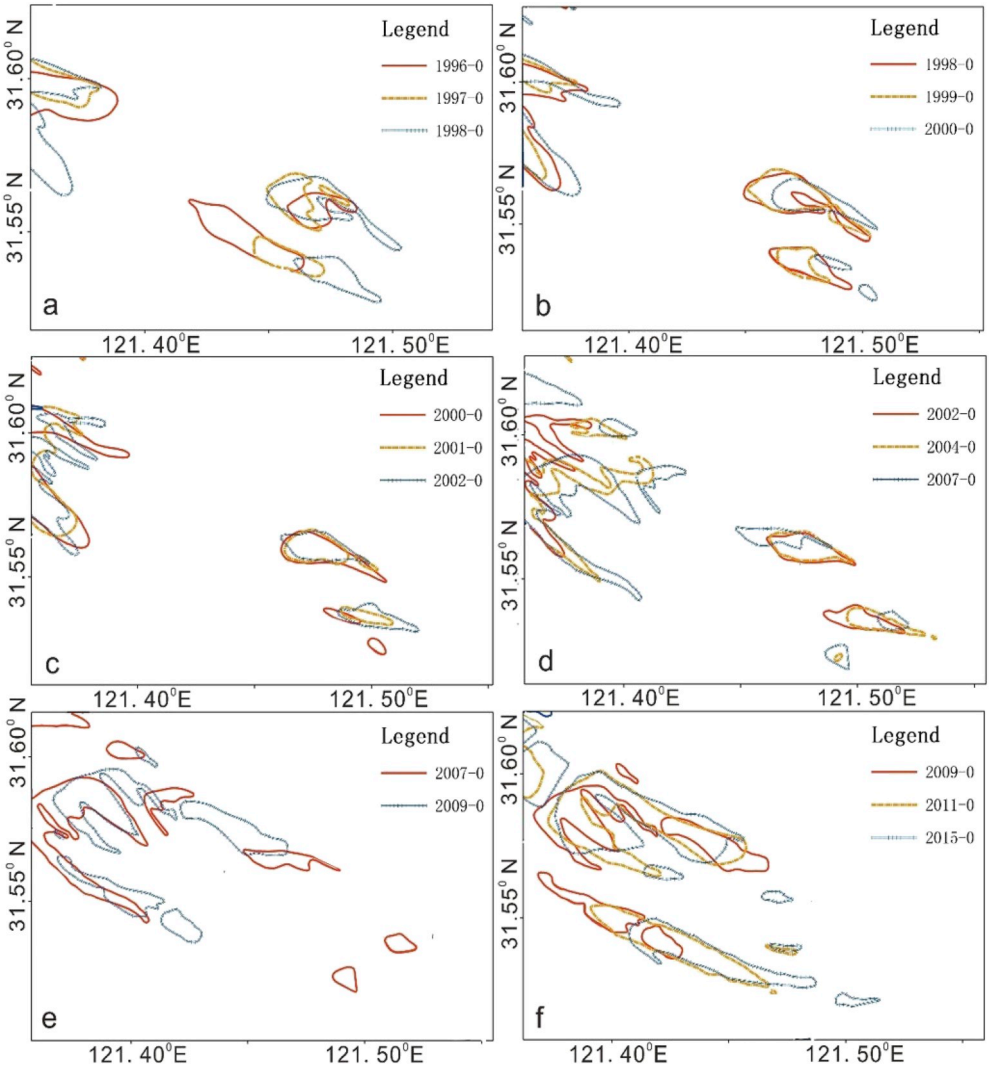

Fig. 3. Temporal evolution of the 0 m isobaths of the BDS-XQC system.

(Fig. 4a–f).

Additionally, the fractal dimension D of the LBDS's 5 m isobaths in different years is exhibited in Fig. 5, which demonstrates a statistically significant upward trend during 1996–2016 ($p < 0.01$). It is worth mentioning that the fractal dimension D was larger than 2 during 2014–2016. This result meant that the contour line of the LBDS tended to be complex, providing further evidence that the LBDS was under a developed condition.

3.2. Morphodynamics of XQC

Unlike the extension of the BDS, the XQC exhibited an obvious decay trend from 1996 to 2016 in volume below 0 m, with an annual volume-decreasing rate of 3.79×10^6 m^3/yr (Fig. 6), indicating that the channel was in a state of accumulation. The surface morphology alterations of the XQC could be reflected by its 10 m isobaths. During 1996–1998, obvious extension appeared at the southern side of the 10 m isobaths, when the isobath head was near Zhangwanggang (Fig. 7a). The area of 10 m isobaths remained invariable from 1998 to 1999. However, in 2000, the head of the 10 m isobaths broke into two parts, with the main part receding by approximately 1.7 km (Fig. 7b). During 2000–2009, there were little variations in the widths of the 10 m isobaths, while the lengths continually developed. Specifically, the upstream separated isobaths continued to enlarge and move upstream, with the head of 10 m isobaths attaching to Nanmengang. The downstream 10 m isobaths retreated by 9 km and moved down to Xinhegang until 2009 (Fig. 7c–e). Meanwhile, this part of the 10 m isobaths shifted from the original shuttle shape with a smooth border to a jagged shape. Furthermore, as the new trough developed (5 m isobaths), the 10 m isobaths of the XQC exhibited the same trend and extended to the LBDS (Fig. 7c–e). During 2009–2014, the 10 m isobaths of the XQC coalesced (Fig. 7f), followed by upward movement and narrowing in the next two years, which meant that the XQC shrank and gradually scoured (Fig. 7f).

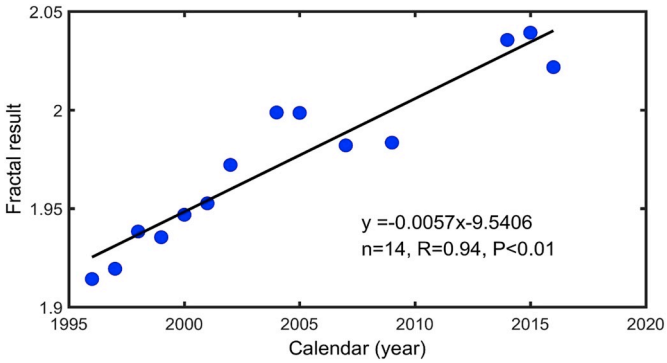

Fig. 5. The fractal result of the BDS contour lines from 1996 to 2016.

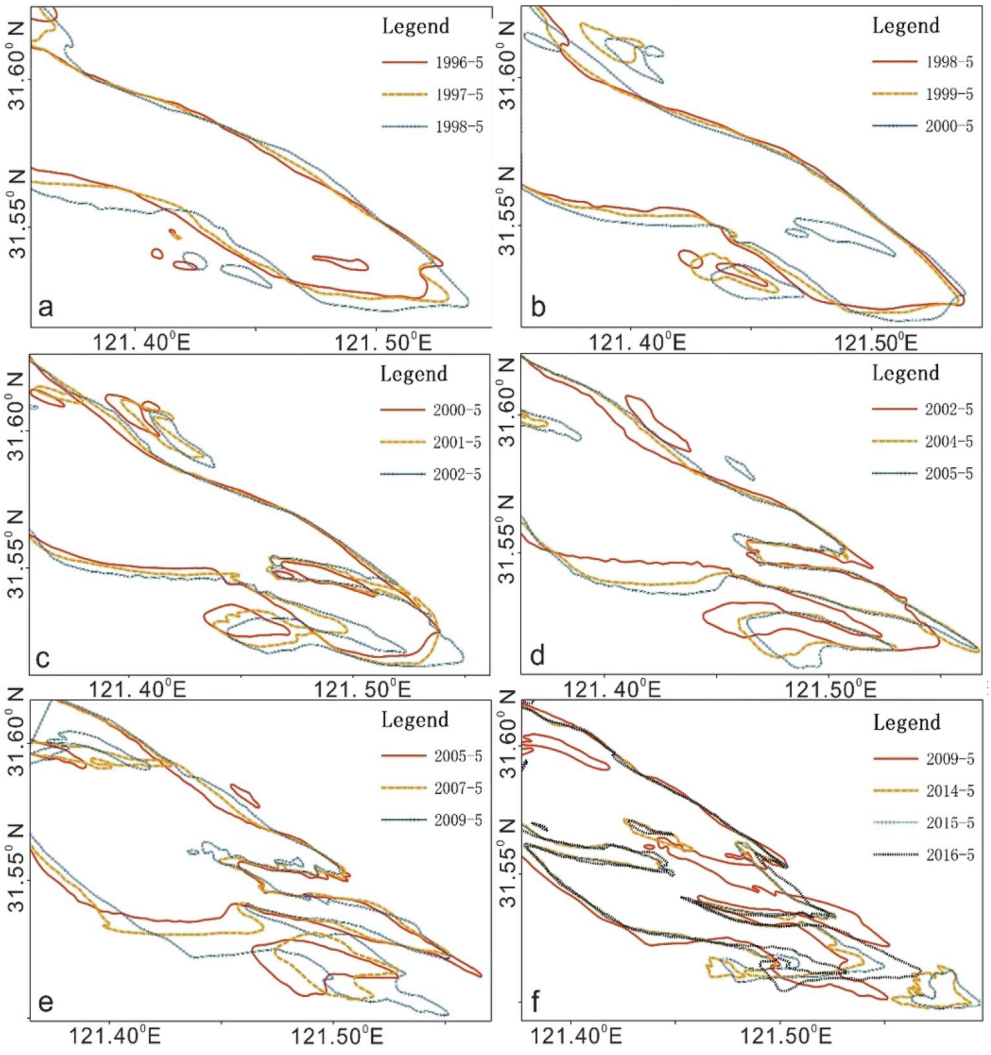

Fig. 4. Temporal evolution of the 5 m isobaths of the BDS-XQC system.

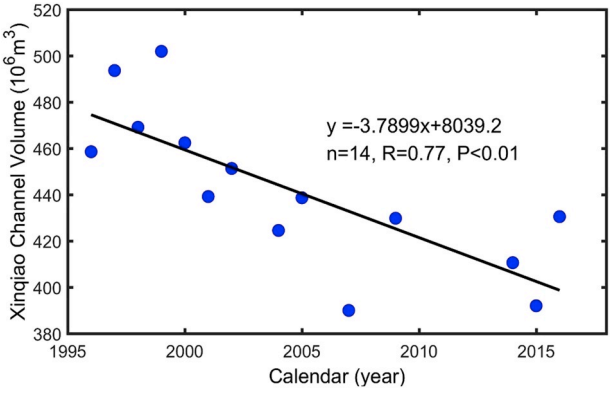

Fig. 6. Volume changes in XQC from 1996 to 2016.

3.3. Geomorphic variations of BDS-XQC system

The cross-sectional variation in the three different transects in correspondence to the upstream, midstream and downstream sections of the BDS-XQC system are shown in Fig. 8. The upstream section of the XQC remained relatively stable during 1996–1997 (Fig. 8a). There was a distinct diminishment of the channel width in 1998, and then the channel became narrower. Specifically, the upstream width of the XQC was approximately 2.1 km in 1996 (Fig. 8a), which, was only 1.1 km in 2016, indicating shrinkage of more than 50% (Fig. 8a). Instead, the width of the LBDS showed an increasing trend from 3.9 km in 1996 to 4.8 km in 2016. In addition, water depth also showed temporal changes in the study period. During 1996–1999, the water depths in the XQC were relatively shallow at approximately 6 m which gradually increased thereafter and reached 10 m in 2009 (Fig. 8a). The water depths in the XQC decreased significantly since 2009 due to severe silting (Fig. 8a). The water depth in the LBDS remained steady from 1996 to 2002. However, an observable cavity occurred in the water depth curve in 2004, when the water depth was reduced to 3–5 m. The curve tried to recover to the original flat state in the following years.

Fig. 8b presents the midstream morphologic variations in the BDS-XQC system. In the horizontal direction, the width of the XQC first increased during 1996–2002, followed by a decrease during 2002–2007, and increased again since 2007. Generally, the width ranged between 1.8 and 2 km, except in 2007, when the channel width was only 1.1 km (Fig. 8b). Similar fluctuations were detected in the midstream of the LBDS, which experienced the processes of narrowing, broadening and narrowing successively from 1996 to 2016. For instance, during 1998–2007, the LBDS continued to expand horizontally, with the width increasing from 3.5 km to 6.4 km (Fig. 8b). Subsequently, it began to shrink as a result of the stretching of the XQC stretching. In the vertical direction, the water depth of the XQC also went through a series of adjustments. The XQC experienced erosion before 1998 when the

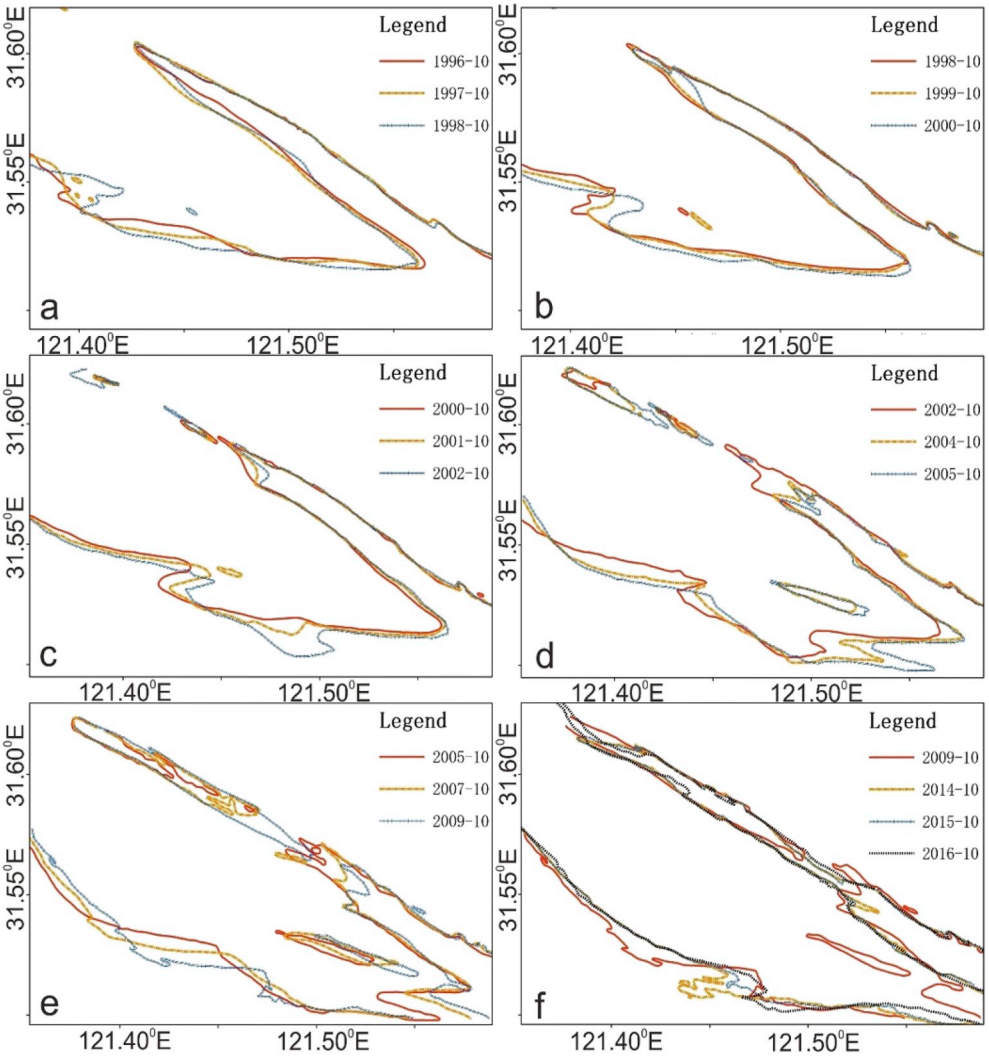

Fig. 7. Temporal evolution of the 10 m isobaths of the BDS-XQC system.

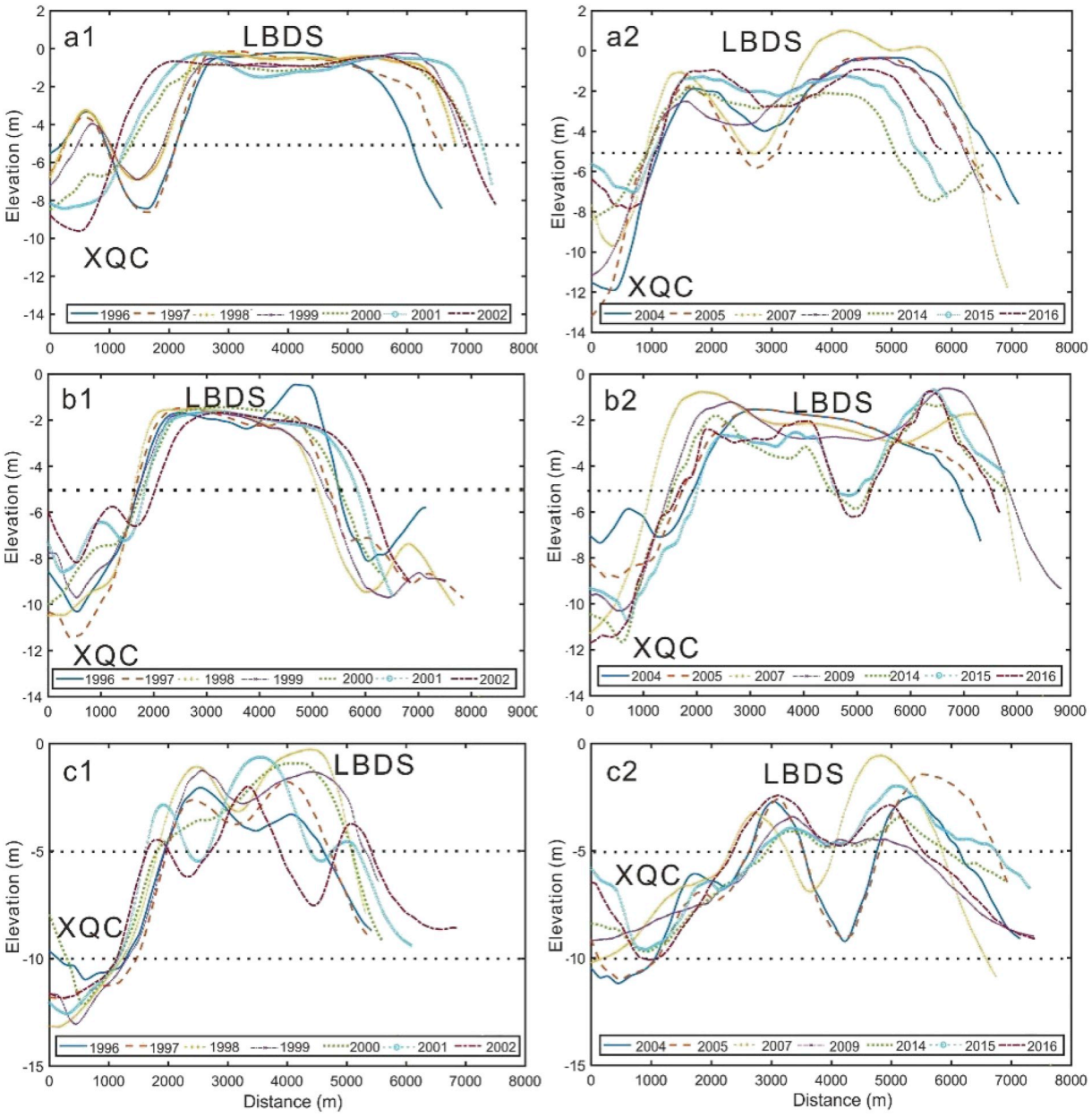

Fig. 8. Temporal bathymetric variations of the Nanmengang section; b Zhangwangang section; c Xinhegang section from 1996 to 2016. The location of each section is shown in Fig. 1c. The dashed lines represent the 5 m and 10 m water depths.

channel depth increased to more than 11 m (Fig. 8b). Then, the XQC entered the silting state until 2004, as the water depths became shallower obviously (Fig. 8b). After 2005, the channel transformed into a scouring state again, with the water depth reaching over 10 m during 2007–2016 (Fig. 8b). The vertical variations in the LBDS, were characterized by the siltation of the shoal's two sides and the development of a trough during 2007–2016 (Fig. 8b).

The evolution of the tail of the BDS-XQC system is shown in Fig. 8c. In contrast to the two upstream sections, the tail part changed more frequently. The width of the XQC decreased from 1.95 km in 1996 to 1.5 km in 2002 (Fig. 8c) and stretched to 2.8 km in 2015 due to the presence of a trough. However, the channel width below a water depth of 10 m exhibited a narrowing trend during 1998–2016. In addition, as the shoal tail changed frequently, the width of the LBDS varied irregularly, with the southern LBDS drifting south similar to the XQC. In the vertical direction, the XQC exhibited siltation during 1998–2016, with the water depth decreasing from 14 m to 10 m (Fig. 8c).

3.4. Erosion and accretion of the BDS-XQC system

The deposition/erosion of the BDS-XQC system could be visualized according to the temporal changes in seafloor elevation (Fig. 9). Between 1996 and 1998, there was obvious erosion in the XQC with a net erosion of 12.8×10^6 m^3/yr, which mainly occurred in the northern XQC where the system bed decreased by 1.5–2.5 m (Fig. 9a), which was accompanied by small-scale depositions near Nanmengang. Meanwhile, the LBDS was in an accumulation state with an accreted volume of 15.5×10^6 m^3/yr. The depocenter of the LBDS was mainly located in the tail section.

During 1998–2009, the XQC changed from an erosion to a silting state, with a mean deposition rate of 2.6×10^6 m^3/yr. There was an obvious erosion area near Nanmengang initially, which gradually expanded and moved downstream (Fig. 9c–k). In addition, a depocenter with a thickness of 0–0.5 m/yr was detected downstream of the erosion area. Meanwhile, the LBDS mainly experienced scouring, except for the

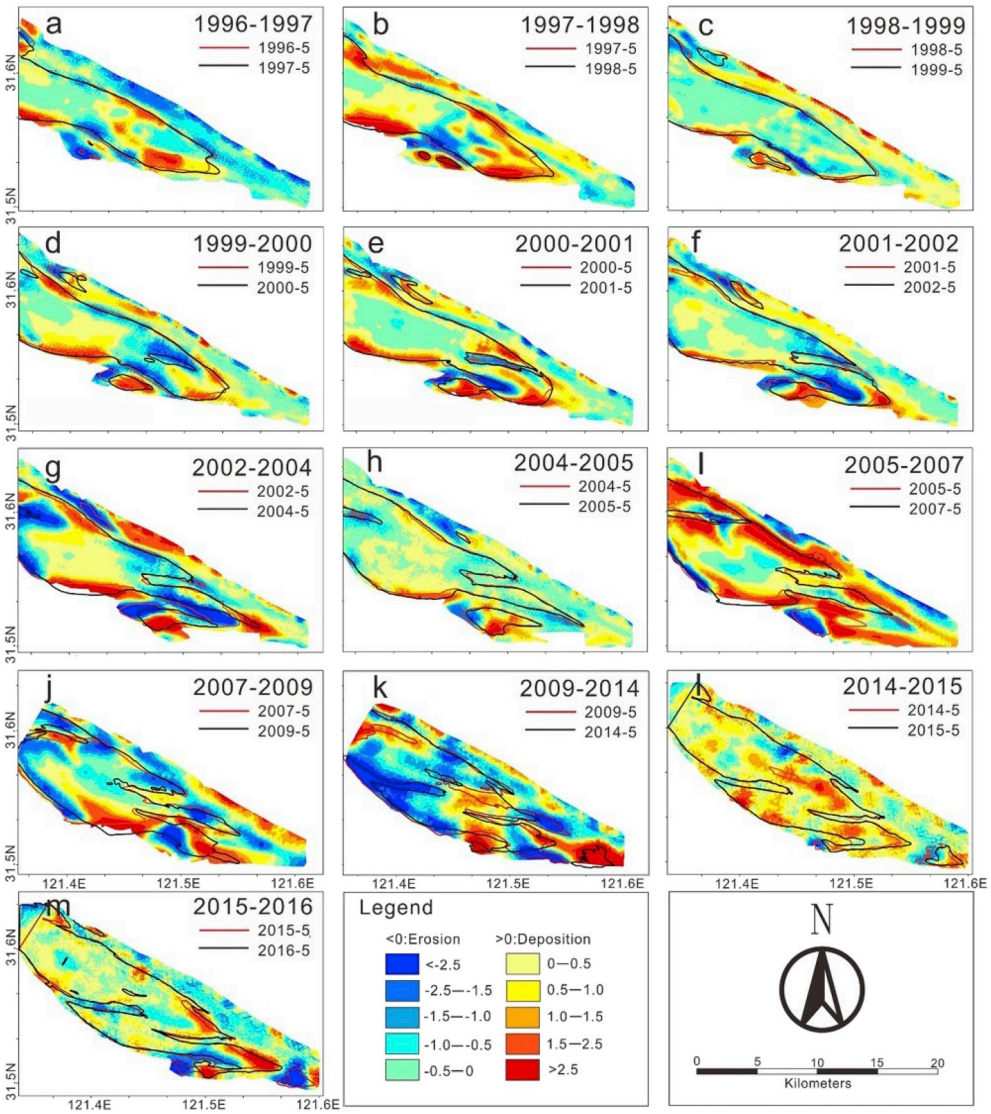

Fig. 9. Yearly erosion/deposition patterns of the BDS-XQC system at nonuniform intervals from 1996 to 2016. Solid lines are the 5 m isobaths depicting the shape of the BDS.

periods of 2000–2001 and 2005–2007. Specifically, strong accumulations were detected around the shoal's border and tail, while strong erosion in the range of 1.5–2.5 m mainly occurred near the troughs and the Xinxinqiao waterway (Fig. 9c–k). Overall, the LBDS was under a slight erosion state with a rate of 1.8×10^6 m^3/yr.

Between 2009 and 2014, the entire BDS-XQC system indicated several erosion periods that were concentrated in the southern portions of the LBDS and XQC. Correspondingly, the volumes of the LBDS and XQC decreased by 8.9×10^6 m^3/yr and increased by 1.3×10^6 m^3/yr, respectively. After 2014, XQC remained the erosion state at a rate of 0.8×10^6 m^3/yr while the LBDS experienced strong accumulation. The mean deposition rate of the LBDS was 30.9×10^6 m^3/yr, with the channel elevation increasing slightly by 0–1 m/yr (Fig. 9l-m).

4. Discussion

4.1. Effect of fluvial water and suspended sediment discharge

In recent decades, the water discharge and SSD from the Changjiang River have changed significantly (Dai et al., 2008, 2018a; Mei et al., 2018b). In particular, following the operation of the Three Gorges Dam in 2003, the annual sediment load in Datong presented a sharp decreasing trend, which decreased by nearly 70% from 1955 to 2016 (Fig. 10) (Yang et al., 2007; Dai et al., 2016). Although there was a plummeting trend of sediment load from the Changjiang River into the estuary, the BDS-XQC system still maintained a state of deposition. Moreover, the LBDS area and XQC volume showed statistically significant ($p < 0.001$) negative and positive correlations with the fluvial sediment load from Changjiang into the estuary in the period from 1996 to 2016 (Fig. 11a2 and b2). The expansion of the BDS and decrease in the volume of the XQC were unrelated to the reduction in the riverine sediment supply. This finding is consistent with the recent work of Dai et al. (2015), who found that the South Passage of the Changjiang Estuary still showed aggradation despite the reduction in the fluvial sediment source (Dai et al., 2015).

In contrast to the sediment load series, the annual discharge through Datong showed statistically insignificant variation from 1950 to 2016 (Fig. 10). Furthermore, there was no visible linear correlation between the BDS-XQC system and the fluvial water discharge (Fig. 11 a1 and b1), indicating that the riverine sediment and water discharge supply were not the factors that directly influenced the evolution of the BDS-XQC system. However, extreme events, such as massive floods, could have an indispensable influence on the evolution of shoal and channel geomorphology (Lane et al., 2007; Nardi and Rinaldi, 2015; Leyland et al.,

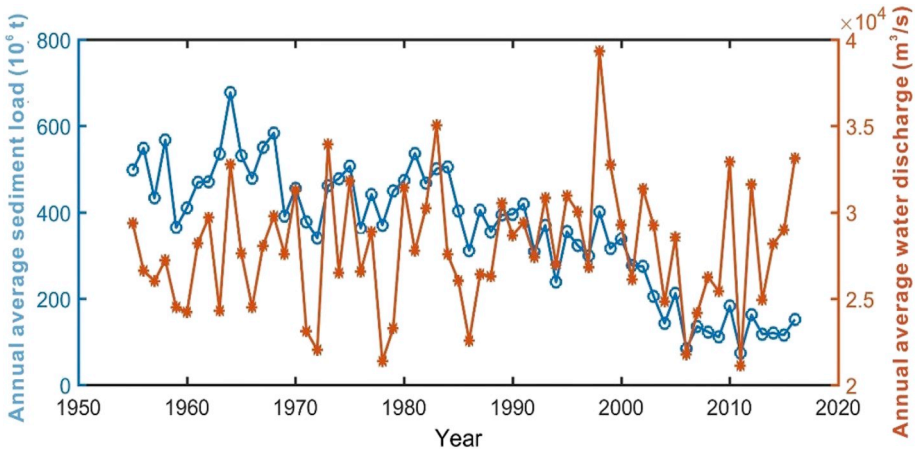

Fig. 10. Average annual discharge and sediment load in Datong station.

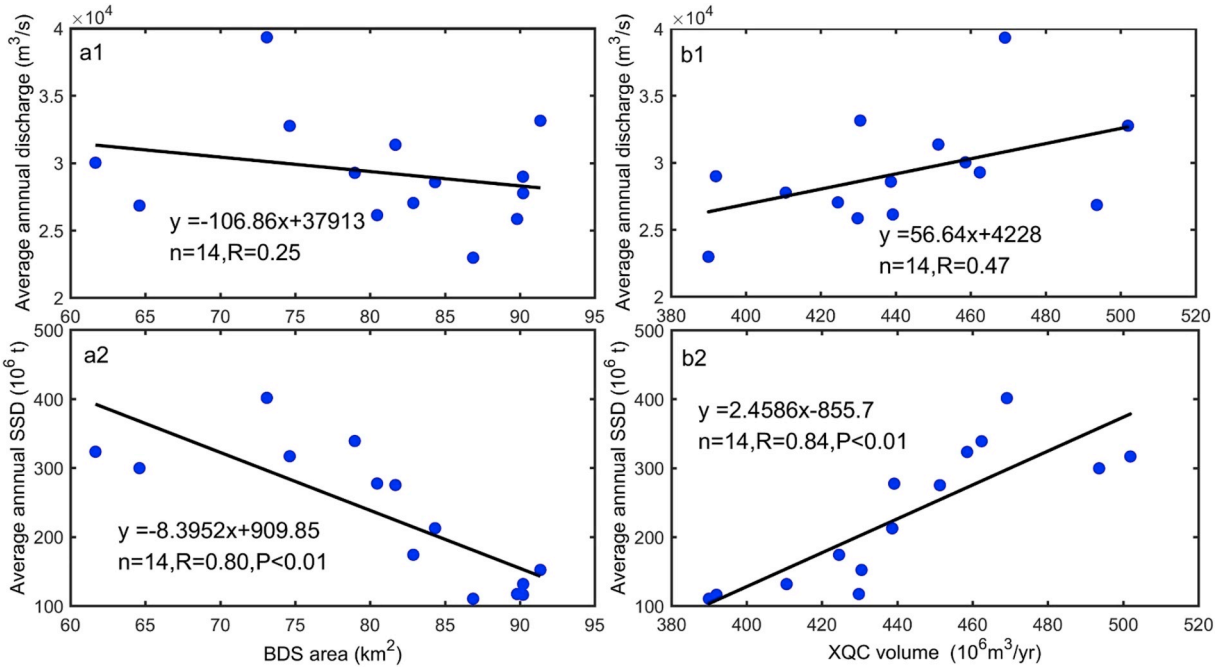

Fig. 11. a The relation between the BDS area and the discharge and SSD in Datong; b the relation between XQC volume and the discharge and SSD in Datong.

2016). During the period from 1996 to 2016, the BDS-XQC system experienced extremely heavy flood disasters in 1998 with the Datong discharge exceeding 7×10^4 m^3/s in July and August (Mei et al., 2018b). Following the 1998 flood, the evolution of the BDS-XQC system transformed from 'shoal deposition and channel erosion' to 'shoal and channel deposition together' (Dou et al., 2011). In particular, the areas of the LBDS above the 0 m and 5 m isobaths increased by 62% and 13%, respectively, while the volume capacity of the XQC declined by 24.5×10^6 m^3 (Figs. 2 and 6). Meanwhile, high discharge with large quantities of sediment during the flood promoted the occurrence of Xinqiao bars around the BDS tail, which further complicated the BDS-XQC system. In addition, the high discharge aggravated the traverse gradient between the South Branch and the XQC, which caused the development of troughs in the LBDS (Hu and Zhan, 2011).

4.2. Effects of local topography and adjacent engineering

Local topography and adjacent engineering have indispensable effects on the morphological evolution of the shoal and channel (Jia et al., 2013). The BDS-XQC system, which is located in the middle reach of the South Branch, is adjacent to the Baimao Shoal. Furthermore, Dongfengxisha Reservoir is located upstream of the system. The existence of Baimao Shoal and Dongfengxisha Reservoir would affect the evolution of the BDS-XQC system (Dou et al., 2011; Xu and Wang, 2015).

Adjacent to the BDS, the river regime of the Baimao Shoal, especially the bifurcation ratio of the North-South Waterway of the Baimao Shoal, may have had a direct influence on the evolution of the BDS. Fig. 12 shows that both the width and the area of the Baimao Shoal North Waterway decreased since 1984, while its ebb tide ratio decreased by nearly 10% during 2002–2012. This result means that the North Waterway of Baimao Shoal was shrinking in recent decades, and the South Waterway was developing correspondingly. These two waterways gradually exhibited a 'south strong and north weak' river regime. Moreover, when the main stream of the South Waterway crossed Qiyakou, a bulgy terrain of the south bank, a deflecting flow phenomenon occurred (Yoshikawa et al., 2007). The main stream shifted northward and scoured the south part of the UBDS, which led to downward sediment transportation. Replenished by the upstream

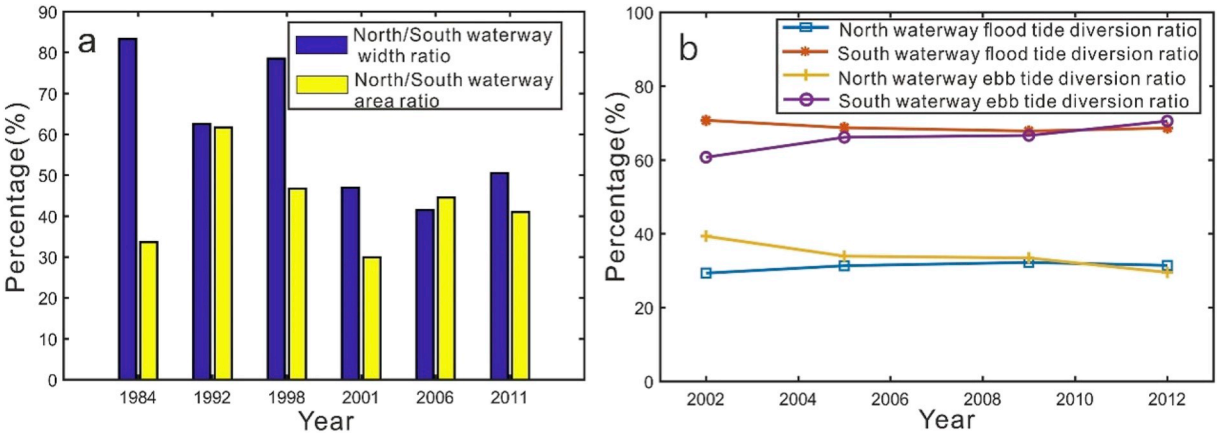

Fig. 12. a The width and area ratios of the Baimao Shoal North/South Waterway; b The flood and ebb tide diversion ratio of the North and South Waterways.

Baimao Shoal sediment, the LBDS expended and moved downward. In addition, due to the extreme flood in 1998, the Baimao Shoal became heavily scoured and moved down, which also provided abundant sediment to the BDS and further promoted LBDS expansion (Xu and Wang, 2015).

With the enhancement of human activities in estuaries, their effects on morphological development may be greater than that of natural forcing factors (Tonis et al., 2002; Klingbeil and Sommerfield, 2005). The adjacent hydraulic engineering plays a vital role in the evolution of the BDS-XQC system. The Dongfengxisha Reservoir, which is located upstream of the BDS, was constructed in 2011 and put into operation in 2014, which significantly affected the system morphology (Fig. 13). Due to the dam interception, upstream flow from the Dongfengxi Shoal was held within the reservoir and had difficulty reaching the XQC. Because the BDS-XQC system belongs to a typical out-bar and inner-stream topography and the XQC is a flood channel, the channel may gradually die out once the upper channel is silted up (Matias et al., 2005). Moreover, the construction of the reservoir hindered the bankfull discharge and SSD from the Dongfengxi Shoal, which raised the shoal elevation and further blocked the trough between the Dongfengxi Shoal and Upper Biandan Shoal. The disappearance of the trough also hindered the entrance of bankfull discharge and SSD of the BDS to the XQC, which caused the silting-up of the sediment on the shoal surface.

Although there is no significant direct relation between the fluvial water and SSD and the evolution of the BDS-XQC system, the local topography and adjacent engineering affect the system development by changing the regional water and SSD. Therefore, it is worth exploring the weight of influences of the discharge, sediment and the system itself on the development of the BDS-XQC system. According to the results of GRA, the annual rate of change in the volume of the XQC was closely related to the erosion/deposition of the BDS, rather than the discharge and SSD in Datong. For the annual rate of change in the volume of the LBDS, discharge in Datong played a primary role, followed by the erosion/deposition of the XQC. It could be deduced that the accumulation in the XQC caused by sedimentation partly stems from the BDS (Table 2). Similarly, the evolution of the BDS was affected by the XQC (Table 3). Additionally, there was a conspicuous linear relationship between the BDS areas and the XQC channel volumes during 1996–2016 as shown in Fig. 14, which meant that the expansion of the LBDS was followed by the shrinking of the XQC.

4.3. Tradeoff between the BDS and XQC

An estuarine geomorphic system always maintains a dynamic equilibrium state (Pacheco et al., 2011; Hu et al., 2018). Therefore, sediment exchanges occurred frequently between the channel and shoal, resulting in a common tradeoff relationship (Dunne et al., 1998; Kleinhans and Berg, 2011). There were also significant interactions between the BDS and XQC. According to the isobaths and erosion/deposition variations of the BDS-XQC system, the system exhibited periodical evolution, which can be further divided into four stages.

Fig. 13. Google Earth images showing the Donfenxisha Reservoir project at different times.

Stage 1 (1996–1998) represents the morphology of the BDS-XQC system before the 1998 flood. Combined with previous studies, we found that this system maintained shoal deposition and channel erosion during 1958–1998 (Yun, 2004; Dou et al., 2011). This evolution trend was also observed on the bathymetric charts from 1996 to 1997 (Fig. 15a). Particularly, elevation changes were concentrated on the margin of the LBDS and XQC, including southward and downward expansion of the LBDS and stretching of the 10 m isobath in the XQC. In

Table 2
Results of grey relational grade for impact factor of XQC volume change.

Year	Average annual volume change rate of XQC (10^6 m^3/yr) (reference sequence)	Average annual sediment load in Datong (10^6 t)	Average annual discharge in Datong (m^3/s)	Average annual depositon/erosion of BDS (10^6 m^3/yr)
1996–1997	35.1	311.3	28425	7.8
1997–1998	−24.5	350.4	33079	23.1
1998–1999	32.8	359.0	36038	−19.5
1999–2000	−39.5	327.7	31008	−9.8
2000–2001	−23.2	308.0	27696	19.9
2001–2002	12.1	276.1	28738	−14.0
2002–2004	−13.4	207.6	28469	−11.5
2004–2005	14.1	177.7	26698	−1.1
2005–2007	−24.3	144.3	24834	26.7
2007–2009	19.9	123.4	25281	−13.0
2009–2014	−3.8	128.1	27367	−8.9
2014–2015	−18.6	118.1	28580	49.5
2015–2016	38.5	134.0	31058	12.3
Grey relational grade		0.574	0.654	0.721

Table 3
Results of grey relational grade for impact factor of BDS volume change.

Year	Average annual volume change rate of BDS (10^6 m^3/yr) (reference sequence)	Average annual sediment load in Datong (10^6 t)	Average annual discharge in Datong (m^3/s)	Average annual depositon/erosion of XQC (10^6 m^3/yr)
1996–1997	2.94	311.3	28425	−36.7
1997–1998	8.50	350.4	33079	11.1
1998–1999	1.53	359.0	36038	13.7
1999–2000	4.34	327.7	31008	1.4
2000–2001	1.49	308.0	27696	−1.9
2001–2002	1.22	276.1	28738	0.3
2002–2004	0.60	207.6	28469	3.3
2004–2005	1.45	177.7	26698	−10.8
2005–2007	1.27	144.3	24834	11.6
2007–2009	1.47	123.4	25281	−1.9
2009–2014	0.08	128.1	27367	−1.3
2014–2015	−0.01	118.1	28580	9.4
2015–2016	1.16	134.0	31058	−10.9
Grey relational grade		0.631	0.674	0.634

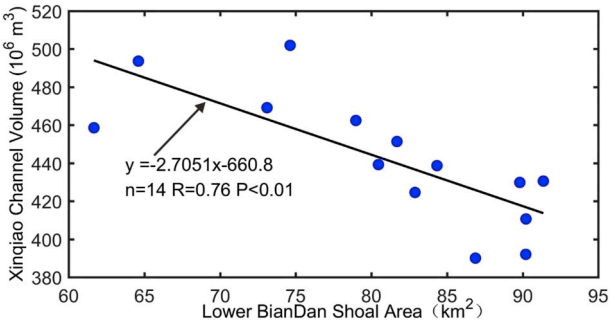

Fig. 14. The linear relation between the LBDS areas and XQC volumes during 1996–2016.

addition, the Nanmen point bar broke and gradually moved downstream (Fig. 15a). Stage 2 (1998–2000) is a conversion stage for the system. Owning to the influence of extreme floods in 1998, the normal status of the BDS-XQC system have been disrupted with dramatic changes. Specifically, the Nanmen point bar nearly scoured out and transformed to a sandbar in the XQC, which moved downstream continuously. Meanwhile, the volume of the LBDS increased significantly by nearly 20% following shoal expansion. However, the stretching of the LBDS hindered the development of the XQC and led to channel narrowing, including decreasing the channel volume and dichotomy of 10 m isobaths of XQC. Other obvious variations in this period were the occurrences of the Xinqiao Shoal, Xinxinqiao Waterway and new troughs in the LBDS (Fig. 15b). Stage 3 (2000–2009) is the extension of Stage 2, when the BDS-XQC system continued to develop. During this phase, the morphodynamics of the LBDS and XQC both experienced obvious variations. Specifically, sandbar in the XQC disappeared because of continuous erosion; the LBDS maintained the expanding and downward trends; the Xinqiao Shoal, Xinxinqiao Waterway and other new troughs continued to develop while the tail of the LBDS gradually evolved into two or three narrow fingerlike sandbars due to the cutting of troughs, which coincided well with the natural sandbar development process as described by Kleinhans et al. (2014). At the same time, 10 m isobaths in the upper and lower sections both extended upstream, showing a significant merging trend. Following the changes in the 10 m isobaths, the XQC exhibited erosion upstream and deposition downstream. Overall, the channel still exhibited a silting up tendency (Fig. 15c). Stage 4 (2009–2016) is a stabilization stage for the BDS-XQC system. During this period, the horizontal expansion of the LBDS slowed, while obvious accretion was distributed on its high flat. The surface morphology of LBDS remained stable. Furthermore, although the Xinqiao Shoal attached to the tail of LBDS and caused the shrinkage of the Xinxinqiao Waterway, the cut-shoal of the LBDS still existed because of the appearance of new troughs. Meanwhile, 10 m isobaths of the XQC eventually coalesced, which tended to stretch upstream and became narrow due to the expansion of the LBDS (Fig. 15d).

4.4. Policies and management of the fragile estuarine CSS system

As valuable freight channels, important water sources for residents and indispensable habitats for organisms, fragile CSS are extremely precious geomorphologic features in estuaries (Hibma et al., 2004; Spalding et al., 2014). Nevertheless, the sensitivity of CSS to external forces makes them unstable and prone to decay. Therefore, there is an urgent need to formulate special management methods and policies for such systems, to promote the sustainable development of system. Particularly, the BDS-XQC is the most obvious developed geomorphic unit in the Changjiang Estuary. Our results demonstrate the linkage of this system through its morphodynamic representations, which are the shoal deposition and channel recession, or the shoal erosion and channel expansion. Thus, when engineering measures are considered for implementation on the shoals to prevent these frequent migrations, the channels' potential variations should not be neglected. This information will help the relevant departments present the corresponding solutions for these morphodynamic shifts. Moreover, our results also illustrate the extreme hydrological events (i.e., extreme floods and droughts) are one of the most important effect factors in inducing abnormal CSS evolutions (Dai et al., 2018b). In light of the impact of extreme hydrological events, a series of monitoring measures are essential to detect CSS changes with the necessary policy to prevent CSS stability from catchment flood impacts. Taken together, CSS are the fragile morphodynamic cells in estuaries with periodic transformations. Hence, in estuary management, it is necessary to follow the evolution of CSS with the adaption of policies based on CSS morphodynamics.

5. Conclusions

As an important geomorphic feature in the South Branch of the Changjiang Estuary, the BDS-XQC system has far-reaching influence on economic development and ecological security in Shanghai. This study explored the evolution of the BDS-XQC system and relevant factors over the past two decades. The main conclusions are as follows:

1. During 1996–2016, the Biandan Shoal (BDS) gradually expanded with an interannual increasing rate of 1.08 km^2, while the Xinqiao

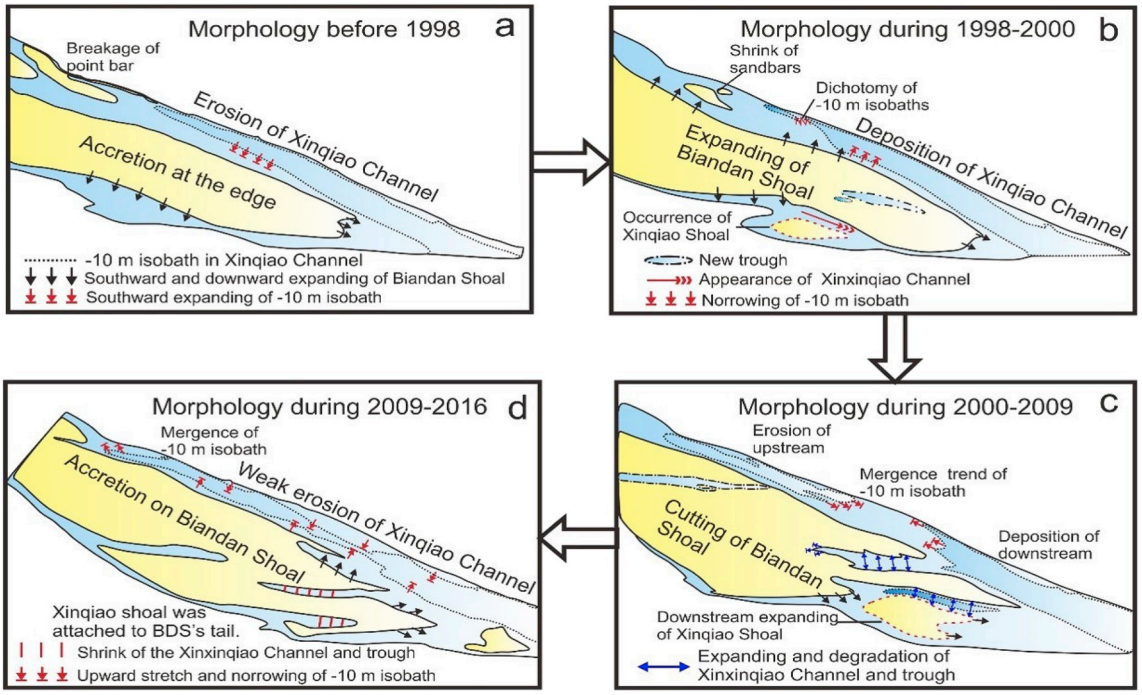

Fig. 15. Conceptual model depicting the morphodynamics of the BDS-XQC system between 1996 and 2016.

Channel (XQC) was transformed from erosion to deposition after 1998. The BDS-XQC depocenter system was mainly located on the tail of the BDS, and strong erosion was concentrated near the troughs.

2. The evolution of the BDS-XQC system during 1996–2016 can be summarized into four stages: Stage 1 (1996–1998) is the preflood phase, revealing shoal deposition and channel erosion. Stage 2 (1998–2000) is the conversion stage because of extreme flooding. Stage 3 (2000–2009) is the development phase with obvious morphodynamic variations in the BDS-XQC system. Stage 4 (2009–2016) is the stabilization stage with high flat deposition of the BDS and continuous shrinking of the XQC.
3. The significant decline in SSD from the Changjiang River has little impact on the changes in the BDS-XQC system, while occasional extreme flooding can alter the system completely. The bifurcation ratio of the North-South Waterway of the Baimao Shoal and Dongfengxisha Reservoir engineering played a vital role in the deposition in the BDS and the decrease in the volume of the XQC. While tradeoffs between the XQC and BDS can maintain the dynamic balance in the BDS-XQC system, weak water discharge into the XQC from the local channel blocked by the construction of the Dongfengxi Reservoir may be responsible for the recession of the XQC.

As discussed in section 4.4, the tradeoff mechanisms of CSS morphological evolution are the key factors that need to be seriously considered during estuary management. Some necessary countermeasures should also consider the sensibilities and phased fluctuations of CSS, which can be significant for creating nature-based estuarine policies and management practices.

Declaration of competing interest

The authors declare no conflict of interest.

Acknowledgments

This study was supported by the Key projects of intergovernmental science and technology innovation cooperation of the Ministry of Science and Technology (2018YFE0109900), International Science and Technology Cooperation Project of Shanghai Science and Technology Commission (19230712400), National Natural Science Foundation of China (NFSC) (41706093) and Academic Capacity Improvement Program for Outstanding Doctoral Students of East China Normal University (40500-20102-222000/003/006).

References

Anthony, E.J., Marriner, N., Morhange, C., 2014. Human influence and the changing geomorphology of Mediterranean deltas and coasts over the last 6000 years: from progradation to destruction phase? Earth Sci. Rev. 139 (5), 336–361.

Barua, D.K., 1990. Suspended sediment movement in the estuary of the Ganges-Brahmaputra-Meghna river system. Mar. Geol. 91 (3), 243–253.

Brake, M.T., Schuttelaars, H.M., 2011. Channel and shoal development in a short tidal embayment: an idealized model study. J. Fluid Mech. 677 (3), 503–529.

Blott, S.J., Pye, K., van der Wal, D., Neal, A., 2006. Long-term morphological change and its causes in the Mersey estuary, NW England. Geomorphology 81 (1–2), 185–206.

Carbonneau, P.E., Lane, S.N., Bergeron, N., 2010. Feature based image processing methods applied to bathymetric measurements from airborne remote sensing in fluvial environments. Earth Surf. Process. Landforms 31 (11), 1413–1423.

Chen, J.Y., Yun, C.X., Xu, H.G., Dong, Y.F., 1979. The developmental model of the ChangJiang River estuary during last 2000 years. Acta Oceanol. Sin. 1, 103–111 (In Chinese with English abstract).

Chen, J.Y., Xu, H.G., 1981. Developmental processes of South Branch channel of Yangtze estuary. J. East China Normal Univ. (Nat. Sci.) 2, 97–112 (In Chinese with English abstract).

Dabees, M.A., Kraus, N.C., 2008. Cumulative effects of channel and ebb shoal dredging on inlet evolution in southwest Florida, USA. In: Proceedings of the 31st International Conference on Coastal Engineering, pp. 2303–2315. Hamburg, Germany.

Dai, S.B., Lu, X.X., Yang, S.L., Cai, A.M., 2008. A preliminary estimate of human and natural contributions to the decline in sediment flux from the Yangtze River to the East China Sea. Quat. Int. 186 (1), 43–54.

Dai, Z.J., Liu, J.T., Wei, W., 2015. Morphological evolution of the south passage in the Changjiang (Yangtze River) estuary, China. Quat. Int. 380, 314–326.

Dai, Z.J., Fagherazzi, S., Mei, X.F., Gao, J., 2016. Decline in suspended sediment concentration delivered by the changjiang (Yangtze) River into the east China sea between 1956 and 2013. Geomorphology 268, 123–132.

Dai, Z.J., Mei, X.F., Stephen, E., Lou, Y.Y., Li, W.H., 2018. Fluvial sediment transfer in the Changjiang (Yangtze) river-estuary depositional system. J. Hydrol. 566, 719–734.

Dai, Z.J., Fagherazzi, S., Gao, S., Mei, X.F., Ge, Z.P., Wei, W., 2018. Scaling properties of estuarine beaches. Mar. Geol. 404, 130–136.

Darby, S.E., Leyland, J., Kummu, M., Rasanen, T.A., Lauri, H., 2013. Decoding the drivers of bank erosion on the Mekong River: the roles of the Asian monsoon, tropical storms, and snowmelt. Water Resour. Res. 49 (4), 2146–2163.

Dunne, T., Mertes, L.A.K., Meade, R.H., Richey, J.E., Forsberg, B.R., 1998. Exchanges of sediment between the flood plain and channel of the Amazon River in Brazil. Geol. Soc. Am. Bull. 110 (4), 31–46.
Dou, X.P., Xia, Y.M., Zhang, X.Z., Xu, X.S., 2011. Analysis on what Influence the Stability of Biandan Sandbank since Appearance of Xuliujing Node, vol. 18. The Fourth Yangtze Forum, Nanjing, pp. 327–334. April.
Dyer, K.R., 1977. Lateral Circulation Effects in Estuaries, In:Estuaries,geophysics and the Environment. National Academy of Sciences, Washington DC, pp. 22–29.
Feder, J., 1988. Fractals. Plenum Press, New York, p. 283.
Hibma, A., Schuttelaars, H.M., Vriend, H.J.D., 2004. Initial formation and long-term evolution of channel–shoal patterns. Cont. Shelf Res. 24 (15), 1637–1650.
Hibma, A., Wang, Z.B., Stive, M.J.F., De, V.H.J., 2008. Modelling impact of dredging and dumping in ebb-flood channel systems. Trans. Tianjin Univ. 14 (4), 271–281.
Hu, H.B., Zhan, Y.L., 2011. Analysis of the evolutional characteristics for a century of South Branch of changjiang estuary supported by GIS. In: Proceedings of the 2011 International Conference on Informatics, Cybernetics, and Computer Engineering (ICCE2011). Springer Berlin Heidelberg, Melbourne, Australia, pp. 331–337, 19–20 November.
Hu, Z., Wal, D.V.D., Cai, H., Belzen, J.V., Bouma, T.J., 2018. Dynamic equilibrium behaviour observed on two contrasting tidal flats from daily monitoring of bed-level changes. Geomorphology 311, 114–126.
Jeuken, M.C.J.L., Wang, Z.B., 2010. Impact of dredging and dumping on the stability of ebb–flood channel systems. Coast. Eng. 57 (6), 553–566.
Jia, L.W., Pan, S.Q., Wu, C.Y., 2013. Effects of the anthropogenic activities on the morphological evolution of the Modaomen estuary, Pearl river delta, China. China Ocean Eng. 27 (6), 795–808.
Kleinhans, M.G., Berg, J.H.V.D., 2011. River channel and bar patterns explained and predicted by an empirical and a physics-based method. Earth Surf. Process. Landforms 36 (6), 721–738.
Kleinhans, M.G., Van Rosmalen, T.M., Roosendaal, C., Van, d.V.M., 2014. Turning the tide: mutually evasive ebb- and flood-dominant channels and bars in an experimental estuary. Adv. Geosci. 39 (39), 21–26.
Kleinhans, M.G., Van Scheltinga, R.T., Maarten, V.D.V., Markies, H., 2015. Turning the tide: growth and dynamics of a tidal basin and inlet in experiments. J. Geophys. Res.: Earth Surf. 120 (1), 95–119.
Klingbeil, D.A., Sommerfield, K.C., 2005. Latest Holocene evolution and human disturbance of a channel segment in the Hudson River Estuary. Mar. Geol. 218, 135–153.
Kuo, Y., Yang, T., Huang, G.W., 2008. The use of grey relational analysis in solving multiple attribute decision-making problems. Comput. Ind. Eng. 55 (1), 80–93.
Lafite, R., Romaña, J.L., 2001. A man-altered macrotidal estuary: the Seine estuary: introduction to the special issue. Estuaries 24 (6B), 939-939.
Lane, S.N., Tayefi, V., Reid, S.C., Yu, D., Hardy, R.J., 2007. Interactions between sediment delivery, channel change, climate change and flood risk in a temperate upland environment. Earth Surf. Process. Landforms 32 (3), 429–446.
Leonardi, N., Kolker, A.S., Fagherazzi, S., 2015. Interplay between river discharge and tides in a delta distributary. Adv. Water Resour. 80, 69–78.
Levinson, A.V., Atkinson, V.L.P., 1999. Spatial gradients in the flow over an estuarine channel. Estuaries 22 (2), 179–193.
Leyland, J., Hackney, C., Darby, S., Parsons, D.R., Best, J., Nicholas, A., Aalto, R., Lague, D., 2016. Extreme flood-driven fluvial bank erosion and sediment loads: direct process measurements using integrated Mobile Laser Scanning (MLS) and hydro-acoustic techniques. Earth Surf. Process. Landforms 42 (2), 334–346.
Liu, G.F., Shen, H.T., Wang, Y.H., Wu, J.X., 2004. Bottom sediment transport in the flood and ebb channels of the changjiang estuary. Mar. Sci. Bull. 6 (1), 88–95.
Liu, J.P., Milliman, J.D., Gao, S., Cheng, P., 2004. Holocene development of the Yellow river's subaqueous delta, north Yellow sea. Mar. Geol. 209 (1), 45–67.
Lopes, R., Betrouni, N., 2009. Fractal and multifractal analysis: a review. Med. Image Anal. 13 (4), 634–649.
Macdonald, I.R., Guinasso, N.L., Reilly, J.F., Brooks, J.M., Callender, W.R., Gabrielle, S. G., 1990. Gulf of Mexico hydrocarbon seep communities: VI. Patterns in community structure and habitat. Geo Mar. Lett. 10 (4), 244–252.
Mandelbrot, B., 1967. How long is the coast of Britain? Statistical self-similarity and fractional dimension. Science 156, 636–638.
Morán, J., Granada, E., Míguez, J.L., Porteiro, J., 2006. Use of grey relational analysis to assess and optimize small biomass boilers. Fuel Process. Technol. 87 (2), 123–127.
Matias, A., Ferreira óscar Mendes, I., Dias, J.A., Vila-Concejo, A., 2005. Artificial construction of dunes in the south of Portugal. J. Coast. Res. 213 (3), 472–481.
Mei, X.F., Dai, Z.J., Wei, W., Li, W.H., Wang, J., Sheng, H., 2018. Secular bathymetric variations of the north channel in the changjiang (Yangtze) estuary, China, 1880–2013: causes and effects. Geomorphology 303, 30–40.
Mei, X.F., Dai, Z.J., Darby, S.E., Gao, S., Wang, J., Jiang, W.G., 2018. Modulation of extreme flood levels by impoundment significantly offset by floodplain loss downstream of the three Gorges dam. Geophys. Res. Lett. 45 (7), 3147–3155.
Nardi, L., Rinaldi, M., 2015. Spatio-temporal patterns of channel changes in response to a major flood event: the case of the Magra River (Central-Northern Italy). Earth Surf. Process. Landforms 40 (3), 326–339.
Pacheco, A., Ferreira, ó, Williams, J.J., 2011. Long-term morphological impacts of the opening of a new inlet on a multiple inlet system. Earth Surf. Process. Landforms 36 (13), 1726–1735.
Rinaldo, Rodriguez-Iturbe, Rigon, Ijjasz-Vasquez, Bras, 1993. Self-organized fractal river networks. Physical review letters 70 (6), 822–830. https://doi.org/10.1103/PhysRevLett.70.822.
Robinson, A.H.W., 1956. The submarine morphology of certain port approach channel systems. J. Navig. 9, 20–46.
Schuttelaars, H.M., De Swart, H.E., 1997. Initial formation of channels and shoals in a short tidal embayment. J. Fluid Mech. 386, 15–42.
Spalding, M.D., Ruffo, S., Lacambra, C., Meliane, I., Hale, L.Z., Shepard, C.C., Beck, M. W., 2014. The role of ecosystems in coastal protection: adapting to climate change and coastal hazards. Ocean Coast Manag. 90, 50–57.
Tonis, I.E., Stam, J.M.T., van de, Graaf J., 2002. Morphological changes of the Haringvliet estuary after closure in 1970. Coast. Eng. 44 (3), 191–203.
Van, d.W.J., Reinders, J., Van Rooijen, A., Holzhauer, H., Ysebaert, T., 2015. Evaluation of a tidal flat sediment nourishment as estuarine management measure. Ocean Coast Manag. 114, 77–87.
Van, d.W.D., Pye, K., 2003. The use of historical bathymetric charts in a GIS to assess morphological change in estuaries. Geogr. J. 169 (1), 21–31.
Van Veen, J., 1950. Ebb and flood channel systems in The Netherlands tidal waters. J. R. Dutch Geogr.Soc. 67, 303–325.
Voorons, M., Germain, M., Benie, G.B., Fung, K., 2003. Segmentation of high resolution images based on the multifractal analysis. In: IEEE International Geoscience and Remote Sensing Symposium, pp. 3531–3533. Toulouse, France, 21-25 July.
Wal, D.V.D., Pye, K., Neal, A., 2002. Long-term morphological change in the Ribble estuary, northwest England. Mar. Geol. 189 (3), 249–266.
Wang, Y.H., Shen, H.T., Li, G.X., Feng, L.G., 2005. Calculation of the amount of siltation and erosion in the Xinqiao Channel of the south Branch of the changjiang estuary in China. Acta Oceanol. Sin. 27 (5), 145–150 (In Chinese with English abstract).
Wang, Y.H., Tang, L.Q., Wang, C.H., Liu, C.J., Dong, Z.D., 2014. Combined effects of channel dredging, land reclamation and long-range jetties upon the long-term evolution of channel-shoal system in Qinzhou Bay, SW China. Ocean Eng. 91, 340–349.
Wei, W., Mei, X.F., Dai, Z.J., Tang, Z.H., 2016. Recent morphodynamic evolution of the largest uninhibited island in the Yangtze (Changjiang) estuary during 1998–2014: influence of the anthropogenic interference. Cont. Shelf Res. 124, 83–94.
Wei, W., Dai, Z.J., Mei, X.F., Liu, J.P., Gao, S., Li, S.S., 2017. Shoal morphodynamics of the Changjiang (Yangtze) estuary: influences from river damming, estuarine hydraulic engineering and reclamation projects. Mar. Geol. 386, 32–43.
Wen, K.L., 2004. The grey system Analysis and its application in gas breakdown and VAR compensator finding (invited paper). Int. J. Comput. Cognit. 2 (1), 21–44.
Xie, D.F., Pan, C.H., 2013. A preliminary study of the turbulence features of the tidal bore in the Qiantang River, China. J. Hydrodyn. Ser. B 25 (6), 903–911.
Xu, J., Wang, J., 2015. Analysis on recent evolution of Baimaosha Branch of Yangtze river estuary. Water Conserv. Sci. Technol. Econ. 21 (11), 86–90 (In Chinese with English abstract).
Yang, S.L., Zhang, J., Xu, X.J., 2007. Influence of the three Gorges dam on downstream delivery of sediment and its environmental implications, Yangtze river. Geophys. Res. Lett. 34, 1–5.
Yoshikawa, H., Ichinomiya, K., Munekata, M., Ohba, H., 2007. Numerical simulation of deflecting flow in a symmetric enlarged channel. J. Therm. Sci. 16 (4), 353–359.
Yu, Q., Wang, Y., Gao, S., Flemming, B., 2012. Modeling the formation of a sand bar within a large funnel-shaped, tide-dominated estuary: Qiantangjiang Estuary, China. Mar. Geol. 299–302 (1), 63–76.
Yun, C.X., 2004. The Recent Evolution of the Changjiang (Yangtze) River Estuary. Ocean Press, Beijing, pp. 115–130 (In Chinese).